

6-1-2012

# Large Eddy Simulation (LES) of Glass Fibre Dispersion in an Internally Spout-Fluidised Bed for Thermoplastic Composite Processing

Xiaogang Yang

*Glyndwr University, x.yang@glyndwr.ac.uk*

Xiaobing Huang

*Glyndwr University, x.huang@glyndwr.ac.uk*


Yuan Zong

*East China University of Science and Technology*

Grance Dai

*East China University of Science and Technology*

Follow this and additional works at: [http://epubs.glyndwr.ac.uk/aer\\_eng](http://epubs.glyndwr.ac.uk/aer_eng)

 Part of the [Aerodynamics and Fluid Mechanics Commons](#), [Complex Fluids Commons](#), [Heat Transfer, Combustion Commons](#), [Manufacturing Commons](#), [Other Materials Science and Engineering Commons](#), [Polymer and Organic Materials Commons](#), [Polymer Science Commons](#), [Process Control and Systems Commons](#), and the [Transport Phenomena Commons](#)

## Recommended Citation

Yang, X., Huang, X., Zong, Y., Dai, G 'Large Eddy Simulation (LES) of Glass Fibre Dispersion in an Internally Spout-Fluidised Bed for Thermoplastic Composite Processing.' [Paper presented to the 2nd International Conference on Advanced Composite Materials and Technologies for Aerospace Applications held at Glyndŵr University, 11-13th June, 2012]. Wrexham: Glyndŵr University.

This Conference Paper is brought to you for free and open access by the Engineering at Glyndŵr University Research Online. It has been accepted for inclusion in Aeronautical Engineering by an authorized administrator of Glyndŵr University Research Online. For more information, please contact [d.jepson@glyndwr.ac.uk](mailto:d.jepson@glyndwr.ac.uk).

---

# Large Eddy Simulation (LES) of Glass Fibre Dispersion in an Internally Spout-Fluidised Bed for Thermoplastic Composite Processing

## Abstract

Large eddy simulation (LES) has been conducted to investigate glass fibre dispersion in an internally spout-fluidised bed with draft tube and disk-baffle, which was used in the manufacture of long glass fibre reinforced thermoplastic composites. The LES results have demonstrated that the internally spout-fluidised bed with draft tube and disk-baffle can remarkably improve its hydrodynamic behaviour, which can effectively disperse fibre bundles and promote pre-impregnation with resin powder in manufacturing fibre reinforced thermoplastics. The hydrodynamics of the spout-fluidised bed has been investigated and reported in a previous paper (Hosseini et al., 2009). This study attempts to reveal important features of fibre dispersion and correlations between the fibre dispersion and the characteristics of turbulence in the internally spout-fluidised bed using the LES modelling, focusing on the likely hydrodynamic impact on fibre dispersion. The simulation has clearly indicated that there exists a strong interaction between the turbulent shear flow and transported fibres in the spout-fluidised bed. Fibre entrainment is strongly correlated with the local vorticity distribution. The dispersion of fibres was modelled by a species transport equation in the LES simulation. The turbulent kinetic energy, Reynolds stress and strain rate were obtained by statistical analysis of the LES results. The LES results also clearly show that addition of the internals in the spout-fluidised bed can significantly change the turbulent flow features and local vorticity distribution, enhancing the capacity and efficiency of fibre flocs dispersion.

## Keywords

Spout-fluidised bed, Fibre flocs, Dispersion, Turbulent flow, LES

## Disciplines

Aerodynamics and Fluid Mechanics | Aerospace Engineering | Chemical Engineering | Complex Fluids | Heat Transfer, Combustion | Manufacturing | Materials Science and Engineering | Other Materials Science and Engineering | Polymer and Organic Materials | Polymer Science | Process Control and Systems | Transport Phenomena

## Comments

Copyright © 2012 Glyndŵr University and the authors, all rights reserved. This article was first presented at the **2nd International Conference on Advanced Composite Materials and Technologies for Aerospace Applications**, June 11-13, 2012, Wrexham, UK and published in the conference proceedings by Glyndŵr University.

Permission to copy, reprint/republish this material for advertising or promotional purposes or for creating new collective works for resale or redistribution must be obtained from Glyndŵr University. By choosing to view this document, you agree to all provisions of the copyright laws protecting it. It is published here with the permission of the Authors, and the full proceedings are available to purchase at <http://www.lulu.com/shop/richard-day-and-sergey-reznik/advanced-composite-materials-and-technologies-for-aerospace-applications/paperback/product-20214156.html;jsessionid=566556BF08A9459FC8807B9BF9878A8D#productDetails>

# Large Eddy Simulation (LES) of Glass Fibre Dispersion in an Internally Spout-Fluidised Bed for Thermoplastic Composite Processing

Xiaogang Yang<sup>1</sup>, Xiaobing Huang<sup>1</sup>, Yuan Zong<sup>2</sup>, Gance Dai<sup>2</sup>

<sup>1</sup> Institute for Art, Science and Technology, Glyndŵr University, Plas Coch, Mold Road, Wrexham, LL11 2AW, UK

<sup>2</sup> State Key Laboratory of Chemical Engineering, East China University of Science and Technology, Shanghai, 200237, P.R.China

**Abstract:** Large eddy simulation (LES) has been conducted to investigate glass fibre dispersion in an internally spout-fluidised bed with draft tube and disk-baffle, which was used in the manufacture of long glass fibre reinforced thermoplastic composites. The LES results have demonstrated that the internally spout-fluidised bed with draft tube and disk-baffle can remarkably improve its hydrodynamic behaviour, which can effectively disperse fibre bundles and promote pre-impregnation with resin powder in manufacturing fibre reinforced thermoplastics. The hydrodynamics of the spout-fluidised bed has been investigated and reported in a previous paper (Hosseini et al., 2009). This study attempts to reveal important features of fibre dispersion and correlations between the fibre dispersion and the characteristics of turbulence in the internally spout-fluidised bed using the LES modelling, focusing on the likely hydrodynamic impact on fibre dispersion. The simulation has clearly indicated that there exists a strong interaction between the turbulent shear flow and transported fibres in the spout-fluidised bed. Fibre entrainment is strongly correlated with the local vorticity distribution. The dispersion of fibres was modelled by a species transport equation in the LES simulation. The turbulent kinetic energy, Reynolds stress and strain rate were obtained by statistical analysis of the LES results. The LES results also clearly show that addition of the internals in the spout-fluidised bed can significantly change the turbulent flow features and local vorticity distribution, enhancing the capacity and efficiency of fibre flocs dispersion.

**Key Words:** Spout-fluidised bed; Fibre flocs; Dispersion; Turbulent flow; LES.

## 1. Introduction

Glass fibre-reinforced thermoplastics have been widely used in different industrial applications. Examples include automotive, airplane, pressure vessels where the use of non-reinforced thermoplastics is unable to provide the specified mechanical and thermal performance. However, high viscosity of thermoplastic and poor dispersion of long fibres imposes many problems in the manufacturing process of thermoplastic composites. A lot of efforts have been made in order to overcome these problems. In order to improve the impregnation with thermoplastic resins, the most attractive techniques that have been developed is to minimise the distance that resin must flow to penetrate the reinforcement. This observation has led to the development of commingled yarns or powder impregnation. The realisation of powder impregnation can be easily achieved using a dry process in which the polymer powders are dispersed through a fluidized bed and are deposited onto the fibre surface by additional force (Padaki and Drzal, 1999). To attain the effective fibre dispersion, additional processing equipment, such as pneumatic spreaders, is usually employed with an increase in production cost.

Dai et al. (2001) proposed the use of the modified spout-fluidised bed to disperse fibre tows and to realise powder impregnation. Using this technology, they have successfully manufactured a new fibre reinforced polymer composite in the laboratory. The aim of this paper is to explore the dispersion mechanism of the fibre flocs in such modified spout-fluidised bed by means of numerical simulation approach (LES) so that the results can provide an essential guidance for optimisation of fibre floc dispersion process. Turbulent flow behaviours in the spout-fluidised bed with different allocations of internals were

investigated using large eddy simulation (LES). The correlations between dispersion of fibre flocs and characteristics of turbulent shear flows were assessed.

Fundamental studies focusing on the conversion of fibre bundles to suspended individual fibres are still rarely reported so far. This may be attributed to the following factors; one is the inherent complexity of fibre flocs, affected by their fragility, coating and physical properties and the other is the complex rupture mode of the fibre flocs (Kuroda and Scott, 2002) caused by surface erosion (gradual shearing off of small fragments from the surface) and large-scale splitting (breakup into fragments of comparable size). There were some applications of fragmentation of flocs in chemical and biological engineering processes, such as protein precipitates (Zumaeta et al., 2007), inorganic nanoparticles (Wengeler and Nirschl, 2007) and colloid particles (Teung et al., 1997) but these fragmentation processes are primarily to depose flocs in turbulent flows using agitated vessels or other process devices. The effect of the turbulent flow field on the fragmented sizes of the flocs has been investigated by Bouyer et al. (2005); Shamlou et al. (1996); Tambo and Hoaumi (1979). These studies have clearly demonstrated that the size of the flocs depends strongly on the interaction between of the flocs cohesion and the shear stress exerted by the turbulent flow on the fibre flocs. These studies also revealed that the fragmentation occurs when the force due to shear stresses is strong enough to overcome the floc cohesion while the flocs withstand when their strength surpasses the shear stresses. It has been widely accepted that the cohesion depends on the physicochemical property of flocs while the features of turbulent flows are mainly controlled by the adopted reactor geometry and operation conditions. As the shear stresses are related to the velocity gradient and turbulence fluctuations, investigations also

revealed that the un-fragmented maximum floc diameter can be correlated to average turbulence dissipation rate or local shear gradient, i.e.  $d \propto \bar{\varepsilon}^{-1/4}$  or  $d \propto G_v^{-1/2}$  (Yeung et al., 1997; Bouyer et al., 2005; Coufourt et al., 2005). Although these empirical relations can be used to qualitatively describe the relationships between the floc size and the hydrodynamics, they cannot provide physical insight into the complex phenomena of fibre floc deagglomeration or break-up in the turbulent flows. In fact, the use of an average turbulence dissipation rate  $e$  to characterise the turbulent shear flow will lead to omission of important details of the local turbulence which is usually crucial for dispersion of fibre flocs. Considering this factor, Ducoste et al. (1997) proposed to correlate the floc size to local shear stress and strain rate. Because the turbulence kinetic energy and dissipation are closely related to shear velocity gradient, it will be reasonable to postulate the floc size to directly correlate to the local shear velocity gradient or vorticity strength. It is evident from the previous studies that fibre floc breakage is likely caused by shear-induced turbulence stresses in turbulent flows (Hosseini et al., 2009), and the final breakage of fibre flocs is dependant upon whether or not the exerted shear stress force is greater than the floc cohesion force.

As turbulent shear stresses have significant impact on dispersion of fibre flocs, deliberate application of turbulence modulation may be effective for controlling dispersion of glass fibre flocs. Spout-fluidised bed has been recognised as an effective means for gas-solid mixing and has been extensively employed in solid drying, coating, blending. Many modifications for spout-fluidised beds have been proposed for improvement of heat transfer and for enhancement of fluid-solid mixing efficiency (Zhou et al., 2004; Zhong et al., 2006) but the use of modified spout-fluidised bed for dispersion of fibre flocs is rarely reported in the open literature. Dai et al. (2001) have proposed the use of modified spout-fluidised bed with a draft tube and a disk-baffle to disperse fibre flocs in the preparation process for manufacturing fibre reinforced thermoplastic composites. It was found that introduction of the internals changes the flow patterns in the modified spout-fluidised bed, resulting in several “sub-flows”, which may be classified as turbulent jet, impinging jet and wall jet. Though these typical flows have been extensively studied and well understood in many previous studies, the superposition of these flows has not been fully investigated. Thus, a better understanding of the hydrodynamics and fibre dispersion in such modified spout-fluidised bed will be beneficial to the control and optimisation of fibre floc dispersion process. Zhong et al. (2006) have adopted Eulerian-Lagrangian CFD modelling approach to study the gas-solid turbulent flow in a spout-fluidised bed. The particle motion was modelled using discrete element method (DEM) while the carrier gas flow was modelled using  $k-\varepsilon$  turbulence model. Wu and Arun (2008) employed Eulerian-Eulerian two fluid model in CFD modelling to simulate the gas-particle flow behaviour of spouted beds and the simulation has quite well predicted the overall flow patterns. Zhao et al. (2008) investigated the dynamics of particulate materials in two-dimensional spouted beds with draft plates by adopting the DEM for describing particle motion and by using the low Reynolds  $k-\varepsilon$  turbulence model for solving for fluid flow. Because the  $k-\varepsilon$  turbu-

lence model was employed in these studies, one of apparent disadvantages is that the details of turbulence structures in the flow were not able to be caught in the simulations. A successful prediction of dispersion of glass fibre flocs requires the details of turbulence structures while it is now generally accepted that large-eddy simulation (LES) can provide the detailed turbulence information except for those dissipated eddies. Thus, the present study has employed the LES to acquire the fluid flow details in the internally spout-fluidised bed. Since fibres with large aspect ratio tend to aggregate and the volume concentration of the glass fibres in the spout-fluidised bed is lower than 0.001% in the operation, the effect of glass fibres on the flow can be neglected, i.e. one-way coupling is assumed. This paper will only consider the effect of the turbulent flow on glass fibre dispersion in the spout-fluidised bed and dispersion of glass fibres is described using scalar transport model, focusing on quantification of the fibre floc dispersion in the spout-fluidised bed.

This paper is organised as follows. Section 2 describes mathematical models and numerical details of the LES employed for simulation of glass fibre dispersion in the internally spout-fluid bed. Section 3 presents the LES simulation results with detailed discussion. Finally, some important conclusions drawn from the present work are given in Section 4.

## 2. Mathematical models and numerical simulation

### 2.1. Flow field and fibre transport descriptions

In LES, the flow variables are decomposed into resolved scales, associated with the larger eddies, and the modelled sub-grid scales, related to the more universal smaller eddies. The resolved scale  $\bar{\phi}$  is obtained utilising a filtering:

$$\bar{\phi}(\mathbf{x}) = \int_D \phi(\mathbf{x}') G(\mathbf{x}, \mathbf{x}') d\mathbf{x}' \quad (1)$$

where  $D$  is the computational domain,  $G$  the filter function, and  $\mathbf{x}$  and  $\mathbf{x}'$  represent the vector positions. The filtered continuity and Navier–Stokes equations on using the previous decomposition and filtering procedure can be written as:

$$\frac{\partial \bar{u}_i}{\partial x_i} = 0 \quad (2)$$

$$\frac{\partial \bar{u}_i}{\partial t} + \frac{\partial}{\partial x_j} (\bar{u}_i \bar{u}_j) = -\frac{1}{\rho} \frac{\partial \bar{p}}{\partial x_i} + \nu \frac{\partial}{\partial x_j} \left( \frac{\partial \bar{u}_i}{\partial x_j} + \frac{\partial \bar{u}_j}{\partial x_i} \right) - \frac{\partial \tau_{ij}}{\partial x_j} \quad (3)$$

where  $\rho$  is the fluid density,  $\tau_{ij} = \overline{u_i u_j} - \bar{u}_i \bar{u}_j$  is the SGS (sub-grid scale) stress, representing the interaction between small and large scales. Smagorinsky (1963) postulated that the SGS stresses  $\tau_{ij}$  can be expressed as

$$\tau_{ij} = 2\nu_T \bar{S}_{ij} \quad (4)$$

where the eddy viscosity  $\nu_T$  and the strain rate in the resolved velocity field are estimated by

$$\nu_T = C \bar{\Delta}^2 |\bar{S}| \quad \bar{S}_{ij} = \frac{\partial \bar{u}_i}{\partial x_j} + \frac{\partial \bar{u}_j}{\partial x_i} \quad (5)$$

where  $\Delta$  is a length scale associated with the filter width (or mesh size) and  $C$  is a constant (Smagorinsky’s con-

stant). In the current study,  $\bar{\Delta} = (\bar{\Delta}_x \bar{\Delta}_y \bar{\Delta}_z)^{1/3}$  and the filter width  $\bar{\Delta}_{x(y,z)}$  is taken the same as the mesh size in the  $x$  ( $y, z$ ) direction. The real flow behaviour of eddies is highly complicated in the internally spout-fluidised bed and the value of  $C$  may be dependent on the local flow behaviour. For simplicity, we have taken  $C = 0.1$  for homogeneous and isotropic turbulence as in Yeh and Lei (1991) and found that this value is reasonable.

In order to describe glass fiber mass transport and dispersion in the spout-fluidised bed, the filtering as defined in equation (1) is applied to the species transport equation used to describe the glass fiber mass concentration, which yields

$$\frac{\partial \rho \tilde{C}}{\partial t} + \frac{\partial}{\partial x_j} (\rho \overline{C u_j}) = \frac{\partial}{\partial x_j} \left( \overline{\rho D_f \frac{\partial C}{\partial x_j}} \right) \quad (6)$$

where  $\tilde{C}$  is the LES grid-resolved species mass. Furthermore, the filtering of the second term in the left side of equation (6) is assumed to take the following form:

$$\rho \overline{C u_j} = \rho \tilde{C} u_j + (\rho \overline{C u_j} - \rho \tilde{C} u_j) \quad (7)$$

The first term on the right hand of equation (7) represents the resolved convective flux of glass fibre mass concentration and the second term can be interpreted as the subgrid scale convective flux (SGS). When adopting the approximation

$$\overline{\rho D_f \frac{\partial C}{\partial x_j}} \approx \rho \tilde{D}_f \frac{\partial \tilde{C}}{\partial x_j}$$

and assuming that the filtered dispersion coefficient is proportional to the carrier fluid viscosity, i.e.

$$\tilde{D}_f = D_f(\tilde{T}, \rho) = \frac{\mu(\tilde{T})}{\rho S c_f}$$

the filtered glass fibre mass concentration transport equation can be written as

$$\frac{\partial \rho \tilde{C}}{\partial t} + \frac{\partial}{\partial x_j} (\rho C u_j) = -\frac{\partial \lambda_f}{\partial x_j} + \frac{\partial}{\partial x_j} \left( \rho D_f \frac{\partial \tilde{C}}{\partial x_j} \right) \quad (8)$$

where  $\lambda_f = \rho \overline{C u_j} - \rho \tilde{C} u_j$ . Solving equation (8) requires a closure model for  $\lambda_f$ . By analogy to decomposition of the flow variables into resolved components and subgrid scale components employed in the large-eddy simulation, the effect of the subgrid scale  $\lambda_f$  is accounted for similar to the Smagorinsky-Lilly model. Since small scales tend to be isotropic, the subgrid scale stress models are based on the eddy-viscosity assumption. Thus, the subgrid term in species glass fibre mass can be approximated by the gradient-transport model, which yields

$$\lambda_f = -\rho \frac{v_t}{S c_i} \frac{\partial \tilde{C}}{\partial x_j} \quad (9)$$

where  $S c_i$  is the turbulent Schmidt number and  $v_t$  is the Smagorinsky viscosity.

It has been found from the LES that the gradients of the mean mass fraction  $C$  in the spout-fluidised bed are small and direct solution of equation (8) yields little information concerning the glass fibre mass variability responsible for flocculation. Of more interest, is the flocculation intensity, as defined by Raghem Moated (1999),

$$Fl = \frac{\overline{(\tilde{C} - \bar{C})^2}}{C_m^2} \quad (10)$$

where  $\bar{C}$  is the time averaged local fibre concentration and  $C_m$  is the average fibre concentration in the whole flow field. The flocculation intensity indicates the level of local mass variability. If there are flocs, the flocculation intensity will be high since glass fibre mass is concentrated in the flocs rather than is distributed between them.

## 2.2. The geometry of the spout-fluid bed and numerical detail

Four different configurations of the spout-fluid bed were considered in the simulation as shown in Fig. 1. The diameter of the bed is 280 mm and its height is 1250 mm. A cone bottom with expansion angle of  $60^\circ$  is mounted to avoid detaining the pockets of stagnated particles. A concentric circular draft tube with internal diameter of 90 mm and length of 700 mm long was fitted to convert the set-up from case A to case B for which the distance between the spout nozzle and the draft tube was kept to 217 mm. When a disk-baffle was installed above the draft tube, the set-up was converted to either case C or case D. The gap between the draft tube and the disk-baffle was kept to 100 mm. The only difference between case C and case D is to consider the effect of rotation. Spouting air directly enters the bed through the spout nozzle while fluidizing air is introduced into the bed via the orifices on the gas distributor. The volumetric flow rate of the spouting gas used in the simulation was  $160 \text{ m}^3/\text{h}$  and that of the fluidizing gas was  $40 \text{ m}^3/\text{h}$ , the same as those used in the experiments. All four configurations were simulated so as to understand the effect of the internals on the flow behaviour in the bed. For simulation of case D, the disk-baffle was assumed to rotate at a speed of 600 rpm.

In the simulations no-slip boundary condition was imposed to the bed walls. The exits of the bed were specified as pressure outlets. The spout nozzle and fluidizing gas distributor were defined as velocity inlets with the specified velocities for spouting gas and fluidizing gas respectively. The disk-baffle in case C was treated as a stationary wall while that in case D was specified as a rotational wall at an angular speed of  $62.83 \text{ rad/s}$ . The pressure-velocity coupling was obtained using SIMPLE algorithm and discretisation scheme for pressure was second order and the scheme for momentum was bounded central differencing. The time step for all cases was kept  $0.0001 \text{ s}$ . The convergence criterions are that for all parameters the residuals were less than  $1 \times 10^{-4}$ . The average grid size was about 3 mm in the simulations. However, a refined mesh with  $Y^+ \approx 5$  in the vicinity of the walls, in consistent with the mesh size requirement for LES, was adopted. A grid dependence check has been conducted with the number of mesh cells doubles compared to the refined mesh but the mesh is uniformly distributed. The trial simulation has indicated that grid invariance of computed results has been ensured. Thus, a mesh system having the refined mesh with  $Y^+ \approx 5$  close to the walls and the average grid size of 3 mm is adopted in all our LES simulations. All the simulations were conducted using the commercial CFD Software Fluent 6.3.26.

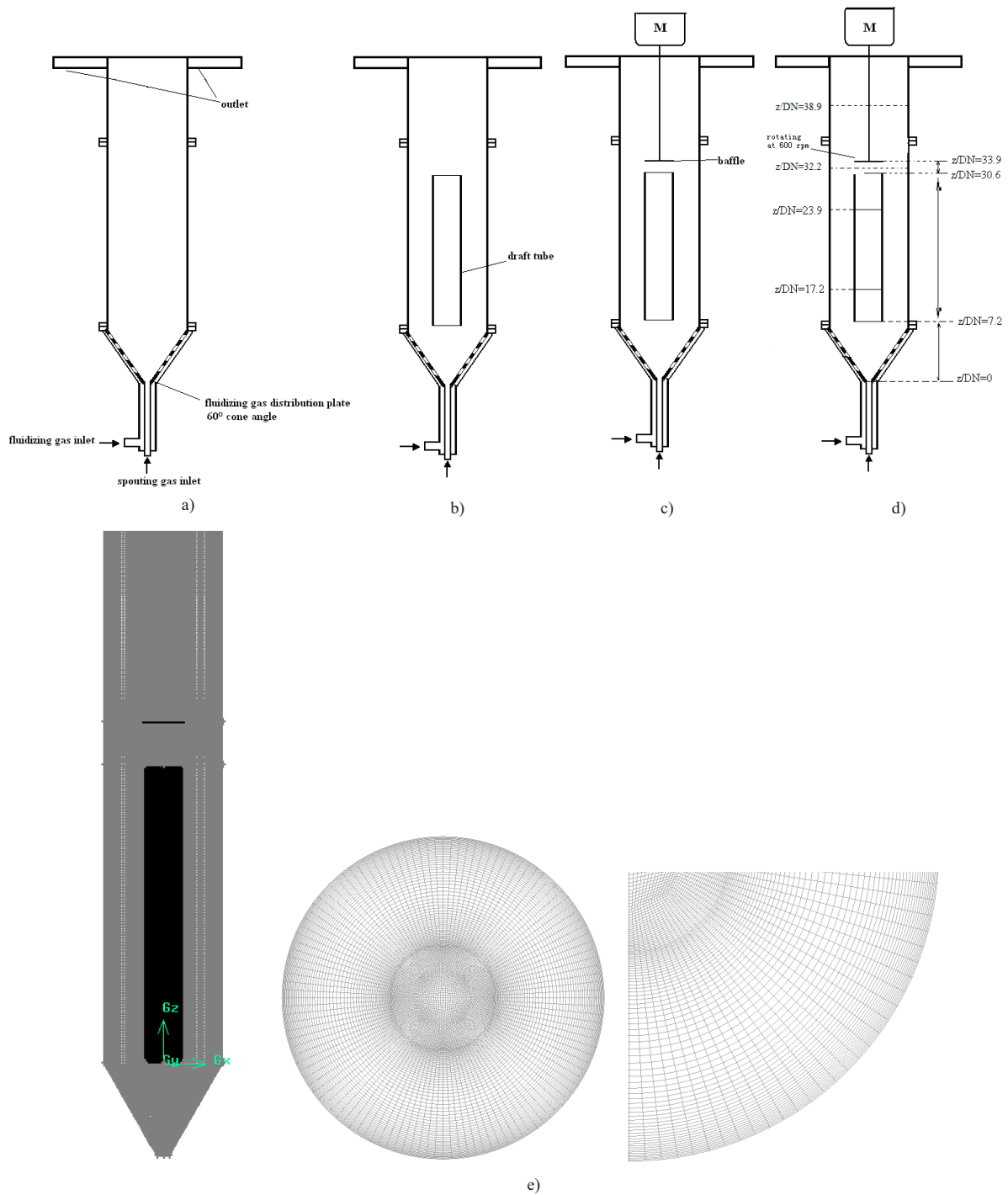


Figure 1. Schematic diagram of four configurations of the spout-fluidised bed used in the simulation: (a) case A; (b) case B; (c) case C; (d) case D; (e) mesh set-up for CFD modelling.

### 3. Results and discussion

#### 3.1. Flow pattern in the spout-fluid beds

Since the volume concentration of the fibres in the spout-fluid bed is lower than 0.001% in the current study, the effect of the glass fibres on the entire flow can be neglected, i.e. only one-way coupling is considered. The LES simulations have been carried out to reveal the turbulent shear flow features in the spout-fluidised bed, in par-

ticular with addition of the draft tube and disk-baffle. In contrast to the previous study on a spouted bed (Wu and Arun, 2008) in which the flow field was characterised to consist of three typical regions, a central spout, an annulus and a fountain region, the current LES results indicate that the turbulent flow in the internally spout-fluidised bed can be dynamically and geometrically characterised with 4 regions. These regions are: (1) the entry region below the draft tube; (2) the annulus located between the draft tube and the walls; (3) the impinging region between

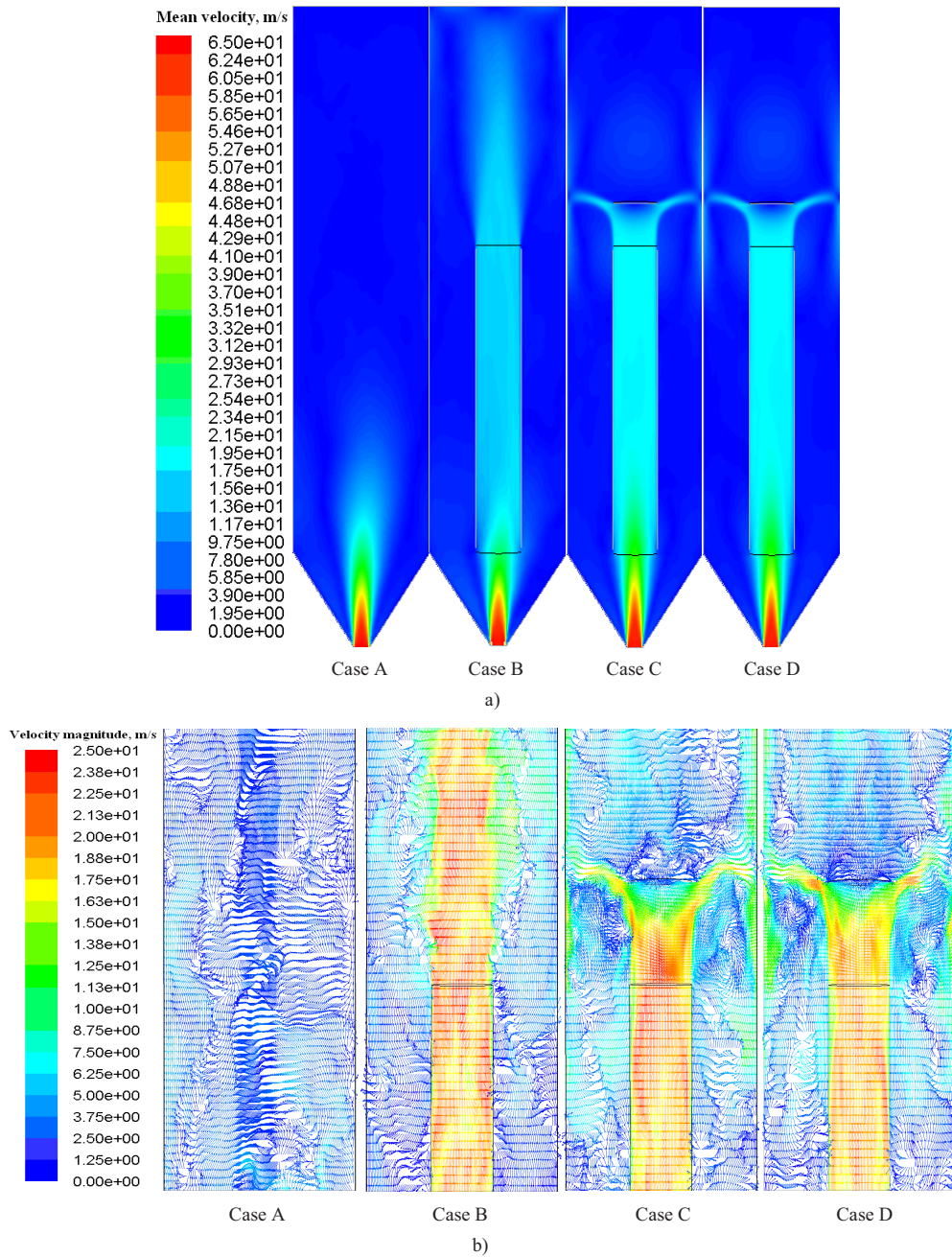


Figure 2. (a) Distribution of the mean flow for all cases; (b) Velocity vector distribution for the impinging and exit region for all cases.  $U_0=65.0$  m/s.

the draft-tube and disk-baffle; and (4) the exit zone above the baffle. Fig. 2(a) showed the time-averaged velocity distribution contours for four different cases. Instantaneous velocity fields in these flow regions are shown in Fig. 2(b). It can be seen clearly from the figure that addition of the internals has a significant impact on the flow behaviour.

### 3.1.1 The entry region and the draft tube

The flow in the entry region of the spout-fluidised bed has typical characteristics of a nozzle jet flow. Introduction of the draft tube has redistributed and modulated the fluid flow, resulting in the presence of relatively regular flow pattern similar to the turbulent shear flow in a circular

tube. Fig. 3 displays the profiles of the axial mean velocity along the centreline and radial mean velocity distributions at different cross-sections for different cases. For case A without the draft tube, the flow can be characterised by jet flow in a confined closure (Moated, 1999). In the early stage of the flow, the jet decays quite quickly and the axial mean velocity on centreline reduces with increase of the axial distance. The length of the potential core of the jet is relatively short. The decay coefficient of the centreline axial mean velocity was found to be 6.94. When draft tube was added, the axial mean velocity decays faster than case A with a decay coefficient of 9.11. This phenomenon was also reported in the previous studies for confined impinging jets, e.g. Ashforth-Frost et al. (1997) and Baydar and Ozmen (2006), which can be at-

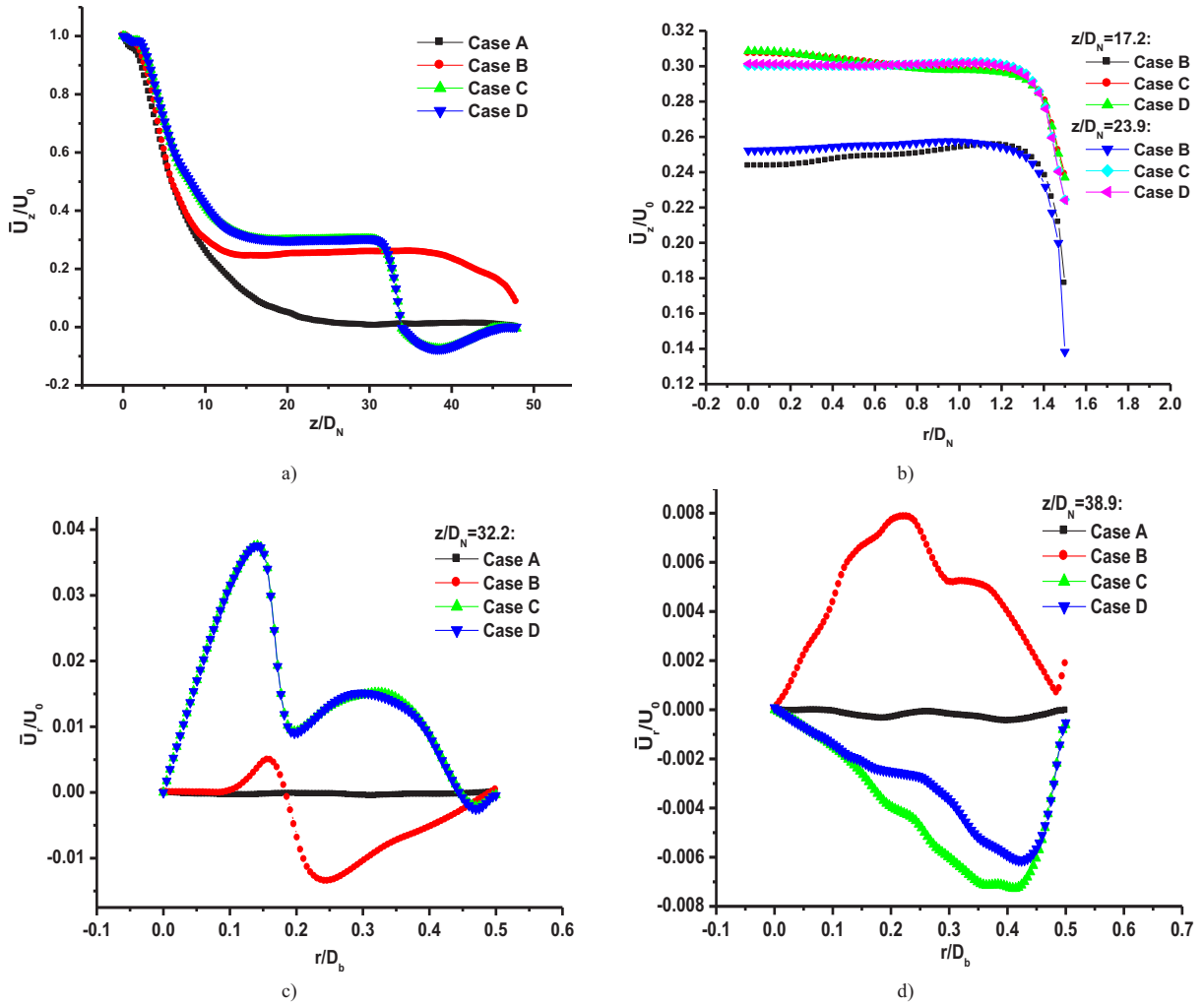


Figure 3. Mean velocity distribution (a) axial mean velocity along the centreline; (b) radial mean velocity distribution at  $z/D_N = 17.2$  and  $z/D_N = 23.9$ ; (c) radial mean velocity distribution at  $z/D_N = 32.2$ ; (d) radial mean velocity at  $z/D_N = 38.9$ .  $U_0 = 65.0$  m/s.

tributed to the confinement on the entrainment and spread of the jet due to the draft tube. The spread of jet flow for case A is only affected by the size of the enclosure while the spread of jet flow for other cases with the draft tube is confined by the draft tube, resulting in the flow to behave similar to the flow through a pipe so that the mean axial velocity remains almost unchanged until the flow leaves the draft tube as shown in Fig. 3(a).

A careful observation on Fig. 3(a) reveals that though the axial mean velocity when the jet flow is led into the draft tube remains unchanged for case B, case C and case D, the axial mean velocity in the draft tube for case B is lower than that for case C and case D. An explanation may be that the presence of the disk-baffle diversifies the outflow from the draft tube and part of the flow has been circulated from the impinging region and entrained into the entry jet, giving rise to a slightly higher axial mean velocity.

### 3.1.2 The annulus and impinging region

The impinging region was defined as the region where the jet flow touches the wall of the spout-fluidised bed. For case A, the jet flow develops initially but forms a pipe flow when the jet flow spreads to touch the wall. For case

B, the turbulent shear flow exiting from the draft tube was forced to change the flow direction due to the disk baffle to form a circular spread jet flow, causing the axial mean velocity variation and sudden change in radial mean velocity distribution at  $z/D_N = 32.2$  (see Fig. 3(a) and (c)). The axial mean velocity distribution on centreline exhibits such behaviour, i.e. keeping unchanged in the draft tube and gradually reducing after the secondary jet flow is generated. Due to the effect of the entrainment of the secondary jet flow, turbulence intensity in the annulus region is enhanced and the axial velocity of the flow in this region increases in comparison to case A.

It was also observed from the simulation that the circular spread impinging jet simultaneously affects the flow behaviour in the annulus region and exit region. As can be seen from Fig. 3(a) that the axial mean velocity reduces steeply. The radial mean velocity increases rapidly from zero at the stagnation point to the maximum at position  $r/D_b \approx 0.15$  and then decreases to a local minimum at  $r/D_b \approx 0.2$ . It increases and attains the second maximum at  $r/D_b \approx 0.3$  and then decreases towards the wall. It is interesting to note that the position of appearance of the first maximum radial mean velocity corresponds to the outer fringe of the disk-baffle. In the formation of the circular spread impinging jet, large-scale toroidal vortices are gener-



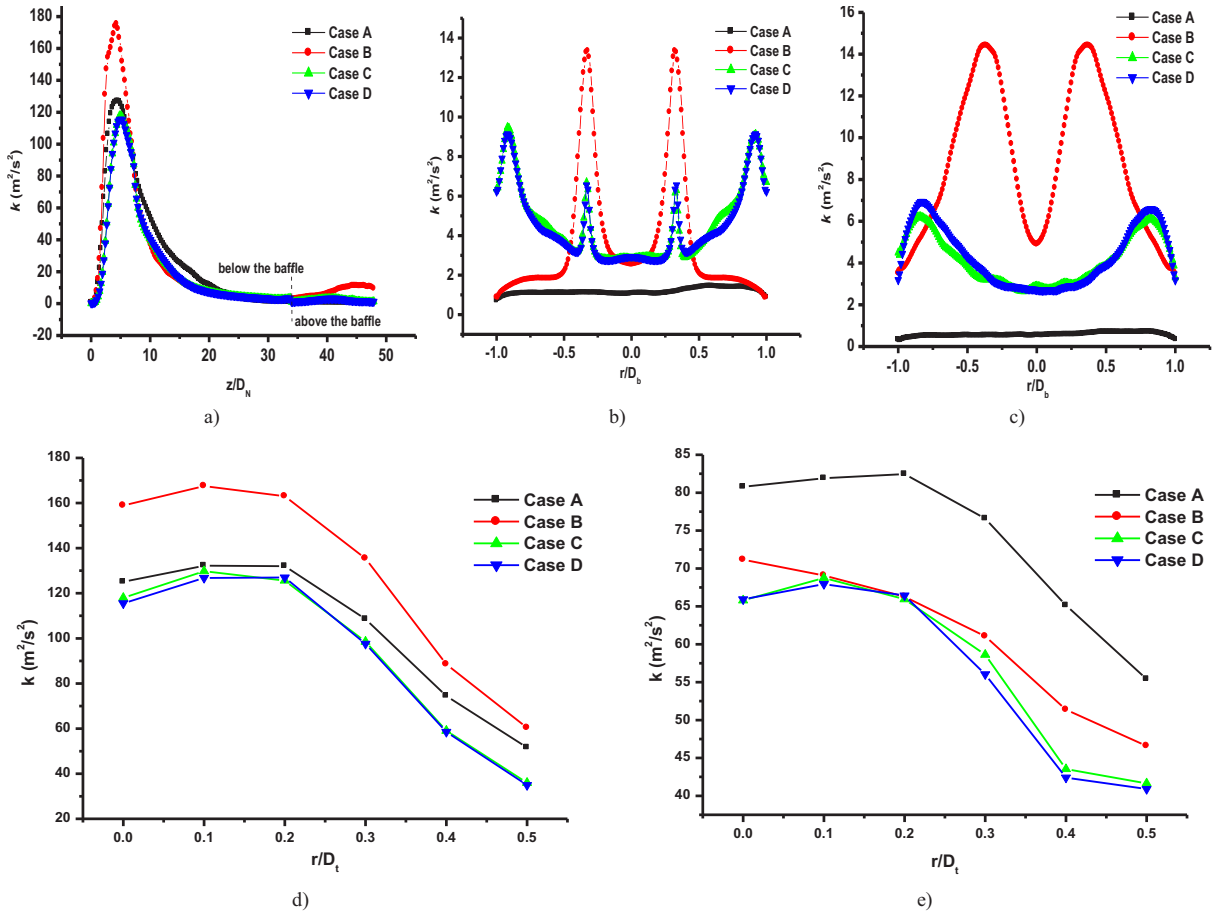


Figure 4. Profile of turbulent kinetic energy at different positions: (a) along the centerline; (b) at  $z/D_N = 32.2$ ; (c) at  $z/D_N = 38.9$ ; (d) at  $z/D_N = 5.0$ ; (e) at  $z/D_N = 7.7$ .

ated respectively on both above and beneath the impinge jet. These two toroidal vortices squeeze the impinge jet so as to form an initial accelerated and then decelerated jet flow, which results in a local maximum radial mean velocity, corresponding to the position of  $r/D_b \approx 0.3$  as can be seen from Fig. 2(b) and Fig. 3(c). Popiel and Trass (1991) indicated that the ring-shaped toroidal vortices formed on the impingement surface would separate from the wall boundary between the stagnation region and wall jet region. Our results seem to be consistent with their finding.

The circular spread impinge jet when hitting the wall generates strong shear both upwards and downwards while the downward shear flow entrains the gas into the annulus and exit regions, intensifying the local turbulence. It was also found that the maximum velocity in the annulus for cases C and D are enhanced to some extent, which is beneficial to fibre floc suspension.

### 3.1.3 The exit region

The strong upward shear flow near the wall in the exit region due to the circular spread impinge jet redistributes and adjusts itself behind the disk baffle. Fig. 3(d) illustrates the profiles of radial mean velocity for all cases in the middle of the exit region ( $z/D_N = 38.9$ ). It can be seen from the figure that the flow for case A in this region has a typical characteristics similar to the fully developed

turbulent flow in a circular pipe, i.e. the radial component of the velocity is almost negligibly small. While for case B, the secondary jet flow from the draft tube has developed quite well at this position and the radial mean velocity profile exhibits the feature of self-preserving which was also confirmed in the previous studies for the confined jet flow. For cases C and D, the upward shear flow (wall jet) along the bed wall is still developing in this region and the flow expands greatly towards the centre of the bed, thus having negative radial velocity component as shown in Fig. 3(d). The upward shear flow also induces huge entrainment and causes a big re-circulation vortex behind the disk-baffle, as can be observed by the existence of two apparent re-circulation vortices almost symmetrical to the centreline.

### 3.2. Turbulence characterisation

Dispersion of flocs depends on interaction between turbulent stresses and floc cohesion force. When turbulence stresses exceed the force for floc cohesion, flocs become disintegrated and dispersed. In the present study, the carrier fluid is air and its viscosity is small so that it is impossible to disperse fibre bundle by viscous shear force. The only feasible way to breakup fibre bundles is to take advantage of the features of turbulent shear flow, i.e. significant enhancement of Reynolds stresses. As the cohesion strength the fibre bundle was obtained by using the

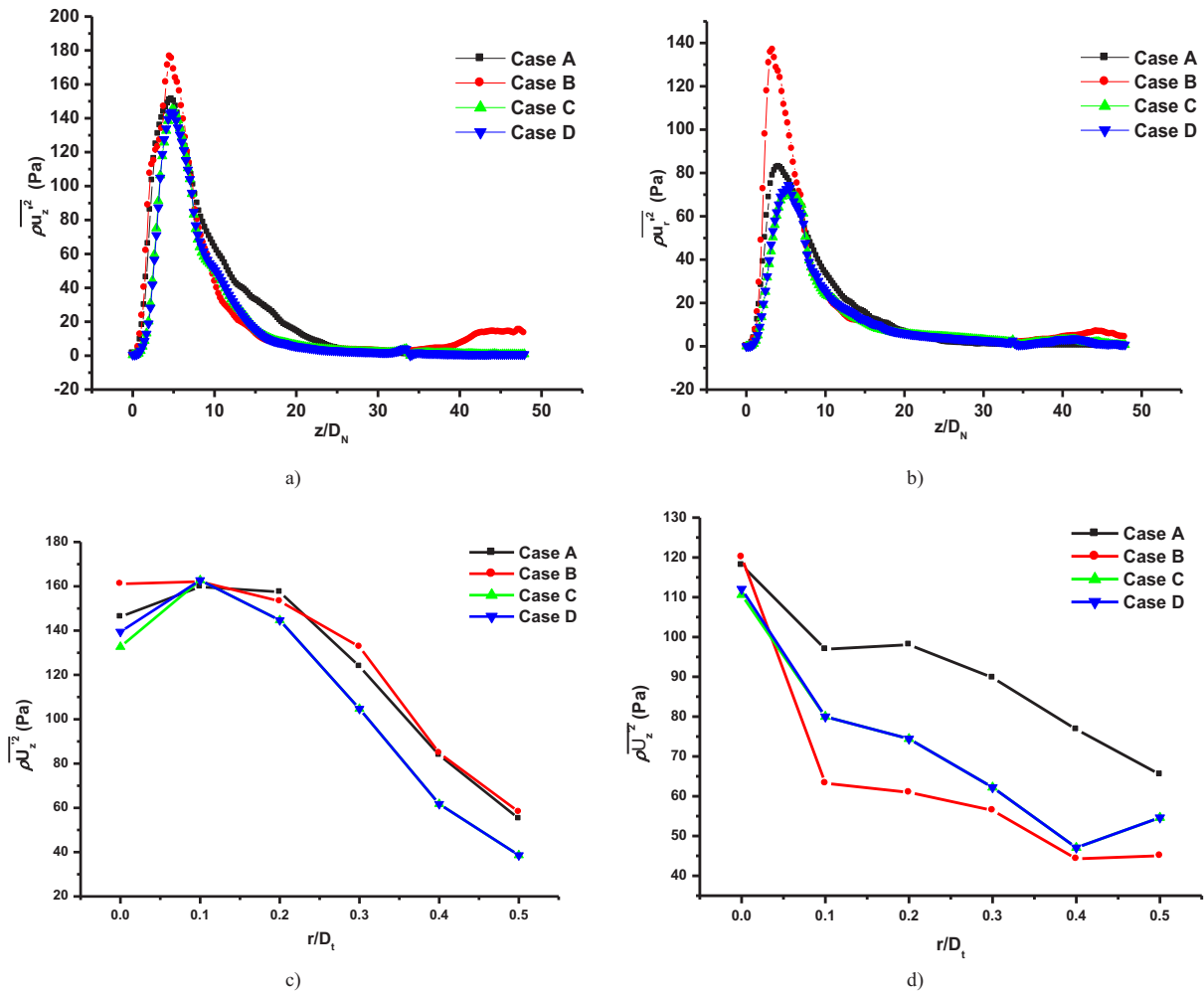


Figure 5. Profiles of normal Reynolds stress variation along the centreline (a)  $\overline{\rho u_z^2}$ ; (b)  $\overline{\rho u_r^2}$ . Profiles of axial normal Reynolds stress  $\overline{\rho U_z^2}$  at two different positions (c) at the entry region  $z/D_N=5.0$ ; (d) in the draft tube  $z/D_N=7.7$ .

rheometer (Zong et al., 2011), it becomes essential to explore whether or not the turbulent stress generated in the turbulent flow in the modified spout-fluidised beds is strong enough to subdue the cohesion strength of the fibre bundle so that fibre flocs can disperse during the flow.

Fig. 4 illustrates the variations of turbulent kinetic energy along the centreline and radial distributions of turbulence kinetic energy at two different cross-sections ( $z/D_N = 32.2$  and  $z/D_N = 38.9$ ) of the bed. Since addition of the internals alters the flow patterns in the bed, it can be seen from the figure that the effect of the internals is remarkable, in particular the draft tube. Without the draft tube, the jet flows from the spouting nozzle, developing strong shear flow in the downstream of the fringe of the nozzle. The shear rate reaches the maximum at  $z/D_N \approx 5$ . This dynamic behaviour can be visualised from Fig. 2 as the ring-shaped vortices generated around the periphery of the nozzle are shedding and spreading, eventually merging to form large scale eddies. Addition of the draft tube confines the spread of shear flow but the shear rate is enhanced as a result of the shear flow to be reinforced in the draft tube. Such turbulence modulation has resulted in a remarkable increase in turbulence kinetic energy as can be seen from Fig. 5. However, introduction of the disk-baffle will restrain the turbulence kinetic energy in the

area between the exit of the draft tube and the disk-baffle, partly associated with a reduction in shear rate, i.e.  $\partial V_z/\partial r$ . For cases C and D, development of the first jet flow from the spouting nozzle is further confined by the circulation formed in the annulus region. Consequently, the turbulent kinetic energy in the entry region slightly decreases as compared with case A (see Fig. 5(a)). It can be also seen from Fig. 5 that the turbulence kinetic energy intensity overall becomes small for case C and case D behind the disk baffle, but the turbulence kinetic energy for case B increases a bit and then decreases. A likely explanation is that the turbulent flow tends to be more uniform downstream of the disk-baffle, where the shear flow of the wall jet has experienced re-development and fewer large eddies are presented as indicated in Fig. 2(b). It is interesting to note that the radial distributions of turbulence kinetic energy at  $z/D_N = 32.2$  for case C and D present bimodal peaks as shown in Fig. 5(b). This behaviour is obviously associated with the shear flow features in the impinge region, where the secondary jet flow exiting from the draft tube is converted to a circular radial impinge jet. The positions of these peaks correspond to the locations with the larger local shear rates. Fig. 5(c) shows that except for case A, all other cases present bimodal peak distribution of the radial turbulence kinetic

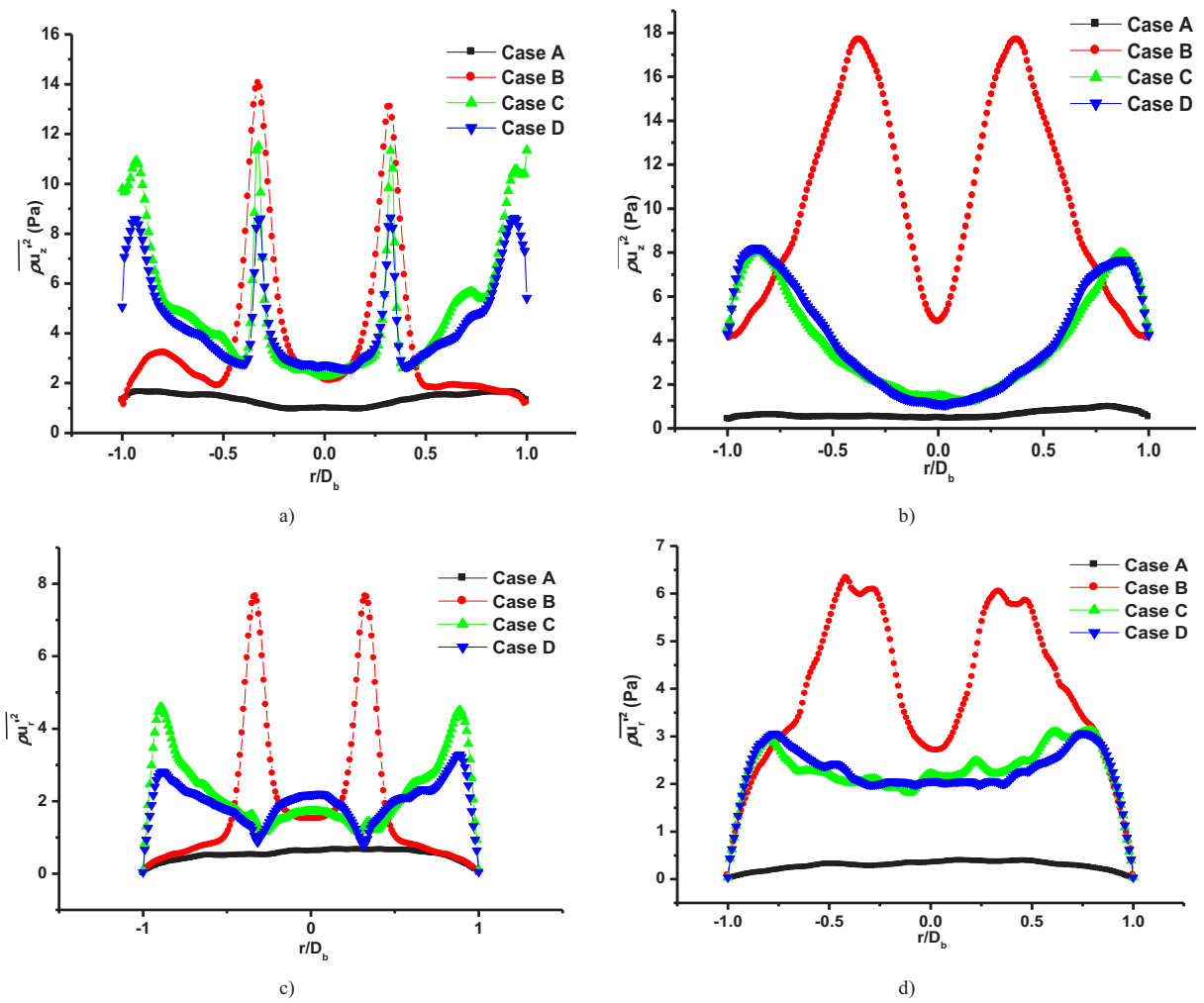


Figure 6. Profiles of normal Reynolds stress: (a)  $\overline{\rho u_z^2}$  at  $z/D_N = 32.2$ ; (b)  $\overline{\rho u_z^2}$  at  $z/D_N = 38.9$ ; (c)  $\overline{\rho u_r^2}$  at  $z/D_N = 32.2$ ; (d)  $\overline{\rho u_r^2}$  at  $z/D_N = 38.9$ .

energy at  $z/D_N = 38.9$ . Among cases with draft tubes, case B exhibits the peak values of turbulence kinetic energy twice times of that for case C and D as a result of strong shear layers formed due to the straightforward secondary jet flow. Due to redistribution of the flow field behind the disk-baffle, the peaks in the turbulence kinetic energy profiles for case C and D have moved towards the wall and their values have been significantly reduced in comparison to case B. This indicates that the shear rates generated by the wall jet (caused by the impinge jet onto the bed wall) in case C and D are smaller. Since turbulence generation is strongly associated with the shear, it implies that the overall shear rate in case B is strongest but this may be harmful for long fibre suspension and transport because the fibres will strongly interact with large eddies.

Fig. 6 illustrates the axial and normal Reynolds stress distributions at cross-sections  $z/D_N = 32.2$  and  $z/D_N = 38.9$  for all four cases while the shear stress  $\overline{\rho u_r u_z}$  contours for all cases are shown in Fig. 7. It can be seen from Fig. 6 that the normal Reynolds stress component  $\overline{\rho u_z^2}$  is much greater than the other Reynolds stress components for all cases with the maximum falling into the entry region. The maximum values achieved in all cases are greater than 140 Pa, which is much higher than the critical

cohesion strength of fibre bundles. This implies that most of fibre bundles will be disintegrated by the turbulent shear flow in the draft tube. For cases C and D, the Reynolds stresses have similar distributions to the turbulence kinetic energy distributions but there exist tiny difference among the profiles. This may be resulted from the effect of rotation of the disk-baffle. At position  $z/D_N = 38.9$ , the profiles of the normal Reynolds stresses  $\overline{\rho u_z^2}$  and  $\overline{\rho u_r^2}$  for both cases are highly similar, i.e. the normal Reynolds stresses increase towards the bed wall, apparently relating to the entrainment effect of the upflowing wall jet. By contrast, the radial normal Reynolds stress in case A is relatively small. Fig. 7 also indicates that the time-averaged resolved shear Reynolds stress distribution is roughly anti-symmetric about the centreline due to the changes of the mean shear rate from positive to negative, which is consistent with the results as reported by Webster et al. (2001) and Beaubert and Viazzo (2003). The sign of the shear stress agrees with the net transport of high momentum away from the centreline. It should be noted here as can be seen from Fig. 7 that the overall magnitudes of the shear stress in case C and case D are lower than that of case B, which may be beneficial to the formation of a relatively uniform fibre floc suspension in the upper part of the spout-fluidised bed.

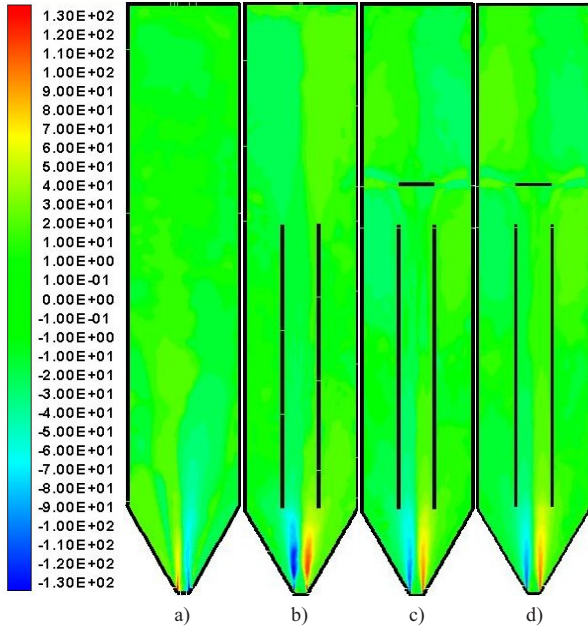


Figure 7. Resolved shear component of Reynolds stress  $\overline{\rho u_i u_j}$ .  
(a) case A; (b) case B; (c) case C; (d) case D.

### 3.3. Correlation between fibre dispersion and local turbulent eddies

It is expected that there exists a strong correlation between glass fibres and turbulent large eddies because turbulent kinetic energy generation is closely related to turbulent eddies. Fig. 9 illustrates the distributions of fibre mass concentration and shears rates in the spout-fluidised bed. It can be seen clearly that those locations with relatively high fibre mass concentration correspond to high vorticity, implying local high kinetic energy generation. The glass fibres are entrained by large turbulent eddies. In order to quantify such correlation, the following correlation is defined to explore this behaviour.

$$\gamma = \frac{\overline{(\tilde{\omega}_i - \bar{\omega}_i)(\tilde{C} - \bar{C})}}{\sqrt{\overline{(\tilde{\omega}_i - \bar{\omega}_i)^2}} \sqrt{\overline{(\tilde{C} - \bar{C})^2}}} \quad (11)$$

Fig. 10 shows the correlation coefficient for fibre mass concentration and local vorticity. It was demonstrated that the correlation coefficient is higher in the regions where the local vorticity is high, as observed in the impinging region in contrast to the entry and exit regions. The maximum  $|\gamma|$  appears in the vicinity of the bed wall at the exit of the disk baffle. The circular spread jet flow generates strong vortices when hitting on the bed wall so that the flocs are entrapped by such eddies and high floc concentration is found in this region (Lin, 2008). The radial distribution of the correlation coefficient shown in Fig. 10(b) further supports this argument.

Fig. 11(a) shows the profiles of  $Fl$  along the axis centerline. It can be seen from the figure that  $Fl$  attains the maximum at inlet of the draft tube ( $z/D_N \approx 4.8$ ) and maintains a relatively greater value along the draft tube. This may be attributed to a strong shear generated by the spouting nozzle, forming large turbulent eddies which entrain the fibres into the draft tube. The fibre flocs/

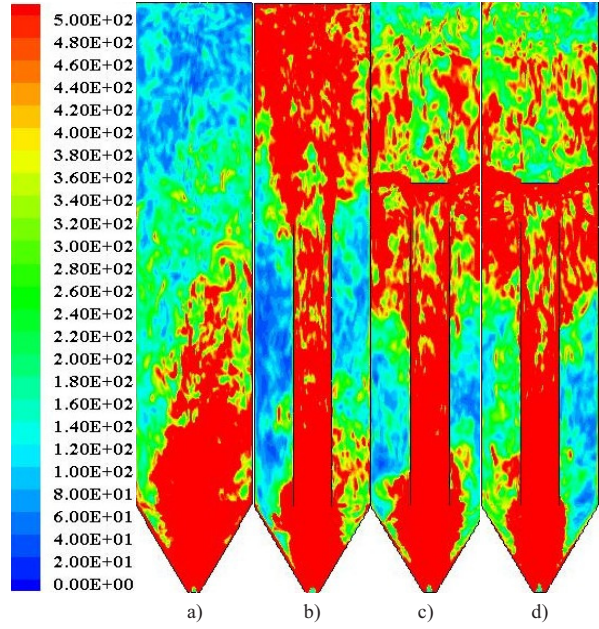


Figure 8. Instantaneous contours of shear strain rate for all cases at  $t = 10$  s: (a) case A; (b) case B; (c) case C; (d) case D. (The shear strain rates ranging from 0 to 500  $s^{-1}$  are displayed only and red represents those values equal to or higher than 500  $s^{-1}$ ).

buddles are apparently influenced by this shear in this stage which is beneficial to floc dispersion. When the flow carries the flocs through the draft tube, dispersion of the fibre flocs/buddles is reduced but  $Fl$  remains almost unchanged until fibres leave the draft tube. Fig. 11(b) illustrates the radial distributions of  $Fl$  at  $z/D_N = 32.23$  and  $z/D_N = 38.9$ , which correspond to the locations of middle impinging jet and exit region respectively. In the impinging region,  $Fl$  reaches the maximum at the centre and the minimum at the location where the circular spread jet just forms.  $Fl$  increases towards the bed wall, indicating the fibres are entrapped by the large eddies formed on the wall. Xu and Aidun (2005) indicated that the size of the flocs directly depends on the interaction between flocs and turbulence intensities in the flow field. When turbulent Reynolds stresses is greater than the cohesion strength of the floc network, disintegration of the flocs is occurring. Otherwise, the flocs may gradually grow. Therefore, the relatively weak turbulence in the jet regime easily causes the formation of the floc while local high vorticity and strong interaction between glass fibres and eddies enhance fibre floc dispersion. In the exit region, the wall jet flow experiences a redistribution process due to the effect of the disk-baffle. The upward shear flow is developing along the bed wall. Owing to formation of vortices with high vorticity, the flocs are entrained these eddies and the local floc mass concentration increases. Thus, how to reasonably control the local vorticity of the turbulent large eddies requires further investigation.

It should be noted here that addition of internals into the spout-fluidised beds is in fact to partition the flow into several sub-flow regions with the hydrodynamic characteristics of either flow contraction or expansion. Blaster (2000) and Kuroda et al. (2002b) have investigated fibre floc deformation in shear and strain flow and their results suggested that the critical mechanical stress required for

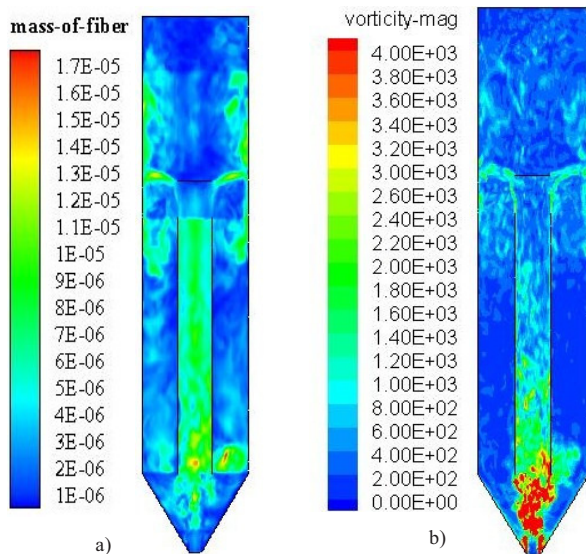


Figure 9. (a) Local fiber mass concentration; (b) local vorticity magnitude ( $|\Omega|^3$   $4000\text{s}^{-1}$  highlighted by 'red').

breaking up the fibre floc depends on types of flows applied and how the fibre flocs are elongated in the flow. A strong shear flow having a local high vorticity is more effective in breaking up droplets and in agglomerating the fibre flocs than a simple shear flow. In this sense, formation of complex turbulent shear flow patterns in the spout-fluid bed by addition of the internals can effectively intensify the vortex stretching due to the formation of different

turbulent eddies so that fibre flocs can be deformed and stretched, further promoting fibre floc dispersion. This is crucial for the case of long fibre flocs to be concerned.

#### 4. Conclusions

The hydrodynamic characteristics of a spout-fluid bed with addition of different internals for purpose of effective dispersion of fibre flocs were studied in this paper. Since fibre floc break-up in shear flows depends to great extent on both floc strength and the features of the applied flow field, fibre floc strength measurements were conducted in a rheometer and the LES simulation of the spout-fluid bed with the internals was carried out to obtain turbulent kinetic energy, Reynolds stress and shear strain rate distributions. Conclusions drawn from the present study are summarised as follows:

- 1) The LES simulation results have shown that addition of the internals (draft tube and disk-baffle) into the spout-fluidised bed can significantly alter the shear flow field, turbulence structures and local vorticity distributions.
- 2) Through controlling the shear flows and effectively enhancing the turbulence intensities, Reynolds stresses can be higher than the strength of fibre flocs coherence so that fibre flocs can be well dispersed.
- 3) Dispersion of fibre flocs benefits from turbulence characteristics in the spout-fluidised bed when internals are effectively utilised.
- 4) LES results clearly indicate existence of a strong correlation between the glass fibre concentration and local

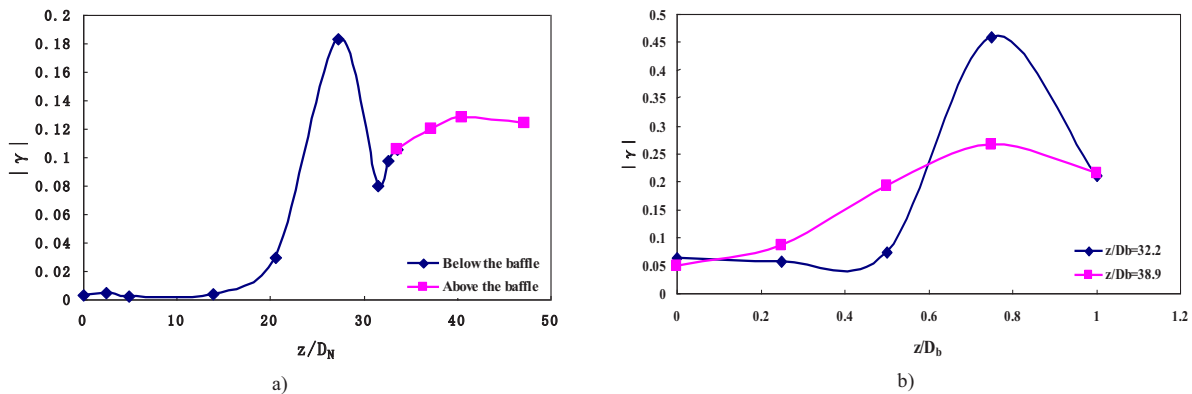


Figure 10. Profile of correlation coefficient  $|\gamma|$  between mass of fiber and local vorticity at different location. (a) axial distribution of  $|\gamma|$  along the centreline; (b) radial distribution of  $|\gamma|$  at  $z/D_b = 32.2$  and  $z/D_b = 38.9$  respectively.

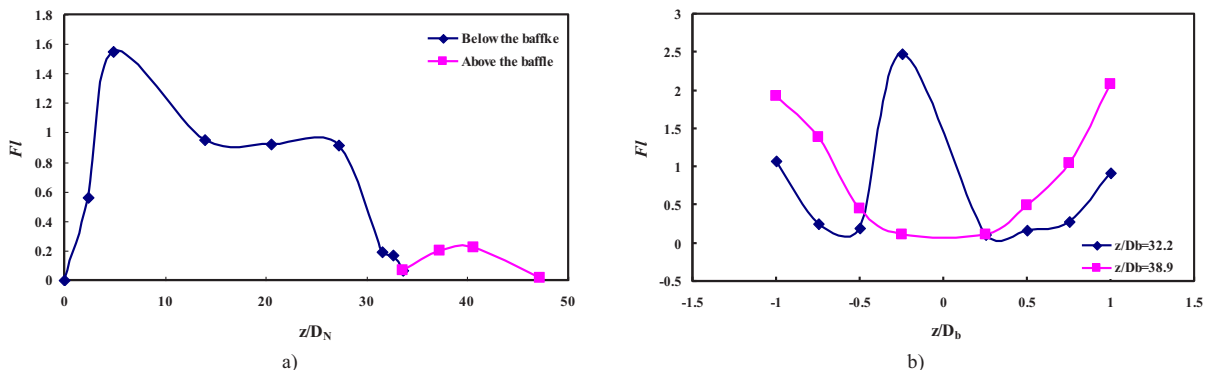


Figure 11. Profile of flocculation intensity ( $FI$ ) at different location. (a) axial distribution of  $FI$  along the centreline; (b) radial distribution of  $FI$  at  $z/D_b = 32.2$  and  $z/D_b = 38.9$  respectively.

vorticity. A local high vorticity corresponds a relatively high glass fibre concentration. The glass fibres are remarkably entrapped by the large eddies.

## 5. Acknowledgement

The authors gratefully acknowledge the support provided by the 111 Project (B08021). Yuan Zong would also like to acknowledge the support of State Key Laboratory of Chemical Reactors, East China University of Science and Technology for a Doctoral programme scholarship. Xiaogang Yang would especially like to thank the support of Glyndŵr University for a Research Fellowship.

## Nomenclature

$C$	Smagorinsky's constant;
$D$	computation domain;
$D_b$	diameter of the spout-fluid bed, m;
$D_d$	diameter of the disk-baffle, m;
$D_N$	the diameter of the spouting nozzle, m;
$D_f$	diameter of draft tube, m;
$G$	the grid filter function;
$G_v$	local velocity gradient, $s^{-1}$ ;
$H$	the distance between disk-baffle and outlet of draft tube, m;
$h$	bob height, mm;
$M$	torque, $m \cdot s$
$U$	mean velocity, $m \cdot s^{-1}$ ;
$U_j$	velocity of the flow at the entrance of draft tube, $m \cdot s^{-1}$ ;
$U_c$	axial mean velocity along centreline, $m \cdot s^{-1}$ ;
$U_0, U_N$	flow velocity at the exit of spouting nozzle, $m \cdot s^{-1}$ ;
$R$	the radius of the spout-fluidised bed, m;
$\bar{S}_{ij}$	resolved scale strain tensor;
$V_r, V_\theta$	radial component and circumferential component;
$d$	floc size, mm;
$k$	turbulent kinetic energy, $m^2 \cdot s^{-3}$ ;
$r$	radius of the baffle, m;
$\bar{u}_i, \bar{u}_j$	the filtered velocity components, $m \cdot s^{-1}$ ;
$u^i, v^i$	fluctuation velocity, $m \cdot s^{-1}$ ;
$X$	axial distance from the nozzle, m;
$x_0$	distance of virtual origin from the nozzle, m.

### Greek letters

$\Omega$	angular velocity, $rad \cdot s^{-1}$ ;
$\alpha$	volume fraction;
$\dot{\gamma}_{bc}$	average shear rate, $s^{-1}$ ;
$\bar{\Delta}$	local mesh size, m;
$e$	turbulence dissipation rate, $m^2 \cdot s^{-3}$ ;
$k$	cup and bob radius ratio, $k = R_c/R_b$ ;
$\eta_T$	eddy viscosity, $Pa \cdot s$ ;
$\rho$	density, $kg \cdot m^{-3}$ ;
$s_{bc}$	average shear stress, $Pa$ ;
$t_{ij}$	sub-grid scale stress, $Pa$ ;
$\omega$	rotational speed, $rad \cdot s^{-1}$ .

### Subscripts

G	gas phase;
F	fibre phase.

## References

Ashforth-Frost, S., Jambunathan, K. and Whitney, C.F. (1997). Velocity and turbulence characteristics of a semiconfined orthogonally impinging slot jet. *Experimental Thermal and Fluid Science*, Vol. 14, pp. 60-67.

Baydar, E. and Ozmen, Y. (2006). An experimental investigation on flow structures of confined and unconfined impinging air jets. *Heat Mass Transfer*, Vol. 42, pp. 338-346.

Beaubert, F. and Viazzo, S. (2003). Large eddy simulations of plane turbulent impinging jets at moderate Reynolds numbers. *International Journal of Heat and Fluid Flow*, Vol. 24, pp. 512-519.

Blaser, S. (2000). Flocs in shear and strain flows. *Journal of Colloid and Interface Science*, Vol. 225, pp. 273-284.

Bouyer, D., Coufort, C., Liné, A. and DoQuang, Z. (2005). Experimental analysis of floc size distributions in a 1-L jar under different hydrodynamics and physicochemical conditions. *Journal of Colloid and Interface Science*, Vol. 292, pp. 413-428.

Coufort, D., Bouyer, D. and Liné, A. (2005). Flocculation related to local hydrodynamics in a Taylor-Couette reactor and in a jar. *Chemical Engineering Science*, Vol. 60, pp. 2179-2192.

Dai, G., Huang, J., Sun, B. and Zhou, X.D. (2001). Agitated-spouted fluidized bed and use in preparing fiber reinforced composite, in: China, 01112947.6 [P], 5-22-2001.

Ducoste, J.J., Clark, M.M. and Weetman, R.J. (1997). Turbulence in flocculators: Effects of tank size and impeller type. *AIChE J.*, Vol. 43, pp. 328-338.

Hosseini, S.H., Zivdar, M. and Rahimi, R. (2009). CFD simulation of gas-solid flow in a spout bed with a non-porous draft tube. *Chemical Engineering and Processing*, Vol. 48, pp. 1539-1548.

Kuroda, M.M.H. and Scott, C.E. (2002a). Initial dispersion mechanisms of chopped glass fibres in polystyrene. *Polymer Composites*, Vol. 23, pp. 395-405.

Kuroda, M.M.H. and Scott, C.E. (2002b). Blade geometry effects on initial dispersion of chopped glass fibres. *Polymer Composites*, Vol. 23, pp. 828-838.

Lin, J. (2008). *Multiphase Fluid Dynamics for Extraordinary Particle Flow-Two Phase Flow with Cylindrical Particles*. Beijing: Science Press.

Moated, R. (1999). *Characterization of Fiber Suspension Flows at Papermaking Consistencies*. PhD Thesis, University of Toronto.

Padaki, S. and Drzal, L.T. (1999). A simulation study on the effects of particle size on the consolidation of polymer powder impregnated tapes. *Composites: Part A*, Vol. 30, pp. 325-337.

Popiel, C.O. and Trass, O. (1991). Visualization of a free and impinging round jet. *Experimental Thermal and Fluid Science*, Vol. 4, pp. 253-264.

Shamlou, P.A., Gierczycki, A.T. and Titchener-Hooker, N.J. (1996). Breakage of flocs in liquid suspensions agitated by vibrating and rotating mixers. *The Chemical Engineering Journal*, Vol. 62, pp. 23-34.

Smagorinsky J. (1963). General circulation experiments with the primitive equations. I. The basic experiment. *Month. Wea. Rev.*, Vol. 91, pp. 99-164.

Tambo, N. and Hozumi, H. (1979). Physical characteristics of flocs - II. Strength of floc. *Water Research*, Vol. 13, pp. 421-427.

Webster, D.R., Roberts, P.J.W. and Ra'ad, L. (2001). Simultaneous DPTV/PLIF measurements of a turbulent jet. *Experiments in Fluids*, Vol. 30, pp. 62-72.

Wengeler, R. and Nirschl, H. (2007). Turbulent hydrodynamic stress induced dispersion and fragmentation of nanoscale agglomerates. *Journal of Colloid and Interface Science*, Vol. 306, pp. 262-273.

Wu, Z. and Arun, S.M. (2008). CFD modelling of the gas-particle flow behavior in spouted beds. *Powder Technology*, Vol. 183, pp. 260-272.

Xu, H. and Aidun, C.K. (2005). Characteristics of fiber suspension flow in a rectangular channel. *International Journal of Multiphase Flow*, Vol. 31, No 3, pp. 318-336.

Yeh, F. and Lei, U. (1991). On the motion of small particles in a homogeneous isotropic turbulent flow. *Phys. Fluids A*, Vol. 3, pp. 2571-2586.

Yeung, A., Gibbs, A. and Pelton, R. (1997). Effect of shear on the strength of polymer-induced flocs. *Journal of Colloid and Interface Science*, Vol. 196, pp. 113-115.

Zhao, X.L., Li, S.Q., Liu, G.Q. and Yao, S.Q. (2008). Flow patterns of solids in a two-dimensional spouted bed with draft plates: PIV measurement and DEM simulations. *Powder Tech.*, Vol. 183, pp. 79-87.

Zhong, W., Xiong, Y., Yuan, Z. and Zhang, M. (2006). DEM simulation of gas-solid flow behaviors in spout-fluid bed. *Chemical Engineering Science*, Vol. 61, pp. 1571-1584.

Zhou, H.S., Flamant, G. and Gauthier D. (2004). DEM-LES of coal combustion in a bubbling fluidized bed. Part I: Gas-particle turbulent flow structure. *Chemical Engineering Science*, Vol. 59, No 20, pp. 4193-4203.

Zong, Y., Yang, X. and Dai, G. (2011). Design simulation of glass-fiber-loaded flow in an internally spout-fluidized bed for processing of thermoplastic composites. I. flow characterization. *Industrial and Engineering Chemistry Research*, Vol. 50, pp. 9181-9196.

Zumaeta, N., Byrne, E.P. and Fitzpatrick, J.J. (2007). Predicting precipitate breakage during turbulent flow through different flow geometries. *Colloids and Surfaces A: Physicochemical and Engineering Aspects*, Vol. 292, pp. 251-263.